2.7 Polarization Studies

The main mission of the polarization studies program is to develop instrumentation and techniques that will utilize the high-brilliance, variably polarized x-ray beam produced from two undulators in sector 4. In addition, this sector will be used for application of x-ray scattering techniques and for high-heat-load testing of front-end components. To briefly review the main operational features, sector 4 has two branch lines, one for the "soft" (0.5 – 3 keV) and the other for the "hard" (> 3 keV) energy range. Variable polarization states will be provided in the soft x-ray regime by a

specialized circularly polarized undulator (CPU), while a planar undulator in combination with crystal optics will be used above 3 keV. A novel concept of spatially separating the beams from the insertion devices was implemented by placing the undulator axes at a small angle (270 μrad) with respect to each other. A dipole electromagnet between the devices introduces the angular deviation of the electron beam, so 30 m away in the first optics enclosure (FOE), the two beams are separated by 8 mm. This is sufficient to use two horizontally deflecting mirrors in the FOE to further separate the beams and direct the soft x-ray beam down the beam pipe. The implementation of this concept enables simultaneous operation of both branch lines and thus more efficient utilization of the delivered beam.

Since the last *Experimental Facilities Division Progress Report* (1998), major milestones have been accomplished. The construction and commissioning of all shielding enclosures were completed. The double-crystal monochromator for the hard x-ray branch was delivered in January of 2000, installed on the beamline in March, and the first monochromatic light was observed on April 1, 2000. Three additional components need to be installed in order to complete the construction of the hard x-ray branch: the phase-retarding tank, scheduled for installation in January of 2001, the focusing mirror chamber in April of 2001, and the flat mirror chamber in July of 2001. For the soft x-ray branch, the installation of horizontally deflecting mirrors and associated vacuum chambers are planned for January of 2001. The entire soft branch will be moved from sector 2 to sector 4 in October as well.

Despite heavy involvement in the construction of sector 4, the development and application of polarization-manipulation-related techniques continued in sector 1 for hard x-rays and, along with spectroscopic techniques, in sector 2 for soft x-rays. Several selected accomplishments are described below. They include characterization and application of a circularly polarized microprobe, temperature-dependent x-ray magnetic circular dichroism on rare-earth compounds, study of interfacial magnetism, exploration of magnetic anisotropy using polarized x–rays, microspectroscopy and imaging with photoelectron microscopy, x-ray-excited optical luminescence studies of oxidized porous silicon, and changes of a ferromagnet/insulator interface upon thermal annealing.

2.7.1 A Microfocused Circularly Polarized X-ray Probe for Energies between 5 and 10 keV

The magnetic contribution to the cross section for scattering of x-rays by matter is of significant scientific interest because of its capability to reveal information about the angular and spin momentum distribution in the scattering medium (Blume and Gibbs, 1988). We report here on a technique that combines microfocusing x-ray optics with Bragg-diffracting phase retarders for producing a circularly polarized x-ray microprobe in the energy range from 5 to 10 keV. Circularly polarized x rays are of particular interest since they couple linearly

to the magnetic moments. A microfocused x-ray beam will enable a wide variety of spatially resolved magnetic scattering experiments, yielding results in applied fields like modern magnetic materials and superconducting compounds, as well as in more basic physics. An important advantage of x-rays in the energy range from 5 to 10 keV is their relatively high penetration power, allowing real bulk measurements of magnetic samples and penetration through nonmagnetic surface layers. Unlike neutrons, x-rays can be used to probe for element-specific properties by working at a particular resonance.

For the energy range between 5 and 10 keV, Bragg-transmission phase retarders have proven to be the most practical approach for the production of a circularly polarized x-ray beam from a linearly polarized synchrotron beam (Hirano et al., 1991). Such phase retarders utilize the fact that, according to the dynamical theory of x-ray diffraction, the wave fields inside a crystal belonging to different linear polarizations propagate with different phase velocities close to a Bragg reflection. The phase difference thus induced is a linear function of the deviation of the angle of incidence from the exact Bragg condition (Lang and Srajer, 1995). Switching the beam helicity requires only minimal rotations of the phase retarder, which can be done even during the course of a measurement, thereby reducing systematic errors. Due to their low absorption, diamond crystals are exceptionally well suited for this application, with only a few crystals of different thickness required to cover the whole energy range between 3 and 12 keV. To produce x-ray beams with submicron cross section, microzone plates are a well-established tool (*X-ray Microscopy and Spectromicroscopy*, 1998). They can be understood as circular diffraction gratings with radially increasing line density, whose operation principle is based on Fresnel's theory of diffracting zones (Born and Wolf, 1980). In the non-diffraction-limited regime, zone plates focus the beam simply by de-magnifying the x-ray source. Since the different diffraction orders of a zone plate correspond to distinct focal lengths, a microfocusing experimental setup typically includes an order-sorting aperture (OSA), e.g., a pinhole, to reduce unwanted diffraction orders. The polarized microprobe was set up at the beamline 1-ID insertion device. Figure 2.69 shows the setup schematically. The undulator beam was collimated using white-beam tungsten slits close to the source. The radiation was then monochromatized using a standard liquid-N_2-cooled double-crystal Si (111) mono-chromator. An additional set of slits downstream of the monochromator was used to further define the beam to a size of 0.5 × 0.5 mm^2 at 60 m from the source. This beam was incident on the phase-retarding optics. For the phase retarder, a 400-µm-thick diamond in (111) reflection geometry was chosen. With an x-ray energy of 8 keV, the incident flux on the diamond was measured to be $\approx 2 \cdot 10^{12}$ photons per second, and the transmitted circularly polarized flux was $4 \cdot 10^{11}$ photons per second. The transmitted radiation had a degree of circular polarization of about 0.99. To suppress higher harmonics, the beam was reflected by a Pd-coated mirror placed behind the phase retarder. The beam path was enclosed in evacuated beam pipes to reduce the intensity loss due to air scattering. The microfocusing setup following the diamond consisted of two parts, the zone plate and the OSA. The

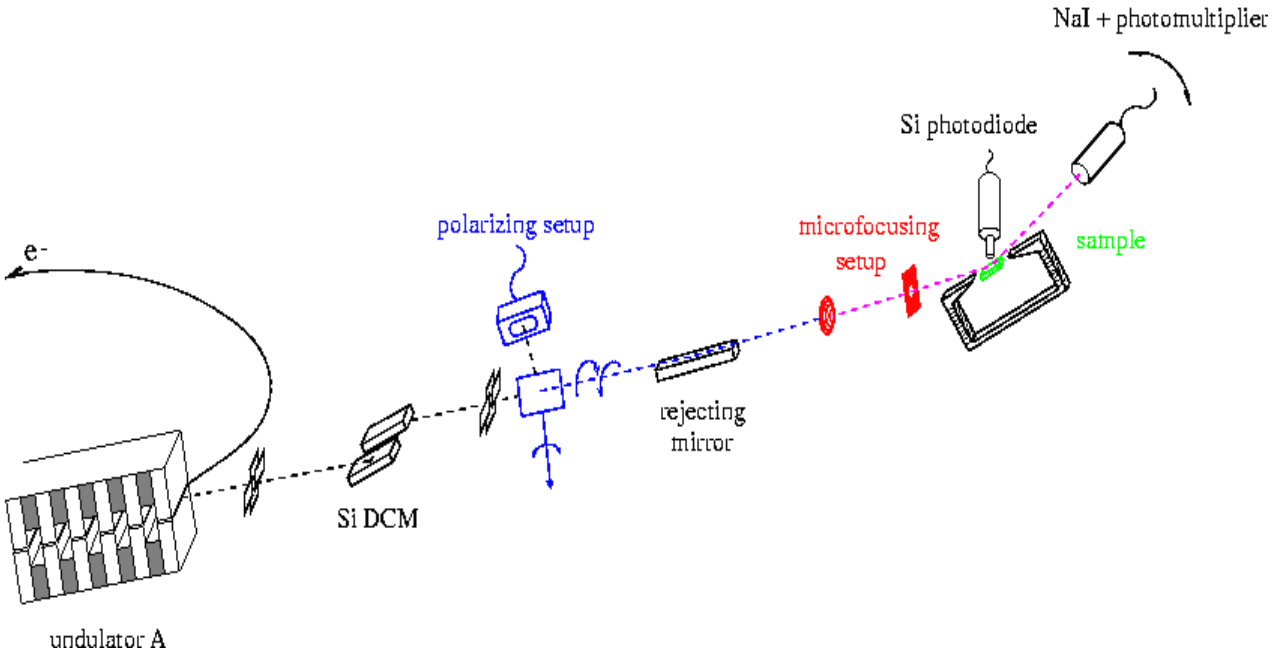

Fig. 2.69. The experimental setup on beamline 1-ID (DCM = double-crystal monochromator).

zone plate had a diameter of 250 µm and a focal length of about 40 cm at 8 keV. It was mounted on a three-axis motorized stage to allow the focused beam to be positioned on the sample. Pinholes of various sizes from 20 to 50 µm were used as order-sorting apertures. The sample was likewise mounted on a three-axis motorized stage in the center of a standard 8-circle diffractometer.

A switchable magnetic field of up to 0.8 T could be applied to the sample parallel to the beam. Two different kinds of detectors were employed to simultaneously monitor both the fluorescence yield and the Bragg-scattered intensity as a function of the position of the sample in the microfocused beam.

The size of the microfocused beam was measured by scanning a Cr-coated knife-edge horizontally and vertically through the beam. The Cr K-fluorescence of the knife-edge was measured as a function of its position in the focused beam. The optimum focus size that could be reached was 4.0×2.3 µm^2 (horiz. × vert.). Horizontally, the measured focus size agrees very well with the value calculated from the demagnification of the source. The vertical size was significantly larger than the calculated value. By temporarily clamping the knife-edge holder on the diffractometer to the zone-plate mounting, we showed that this difference is mainly due to vibrations of the knife-edge relative to the zone plate. For the mentioned focal size, we measured a flux on the order of 10^8 photons per second (Pollmann et al., 2000).

As a demonstration experiment, we used the microprobe to image magnetic domains in a $HoFe_2$ crystal at the Ho L_3 edge. Observing the (400) Bragg reflection of the crystal, two-dimensional scans were performed while reversing the helicity of the incident

beam to obtain the flipping ratio for each point on the sample. The flipping ratio is defined as the normalized intensity difference for orthogonal polarizations of the incident x-ray beam.

Figure 2.70 shows two such mappings of the flipping ratio that were obtained with oppositely oriented applied magnetic fields. The reorientation of the local magnetic moments when the field was reversed can be seen in the reversal of the sign of the measured flipping ratio.

Figure 2.71 shows the remanent magnetic structure of the $HoFe_2$ crystal, as measured without an applied field. In this case, a clear contrast of the measured flipping ratio at different regions of the sample can be discerned. These regions can be identified as different magnetic domains. Their size matched previous results obtained by magnetic force microscopy measurements (Srajer et al., unpublished).

In summary, we built a circularly polarized x-ray microprobe with a high degree of polarization and small beam cross section. The beam was polarized by means of a diamond phase retarder. The obtained degree of polarization was up to 99%. The polarized beam was focused using a microzone plate. The useful beam spot had a size of about 4 × 2 μm. The setup can be used to perform magnetic domain mapping measurements on materials like spring magnets or magnetic multilayers. To improve the spatial resolution, the use of a microzone plate with smaller zone structure is planned.

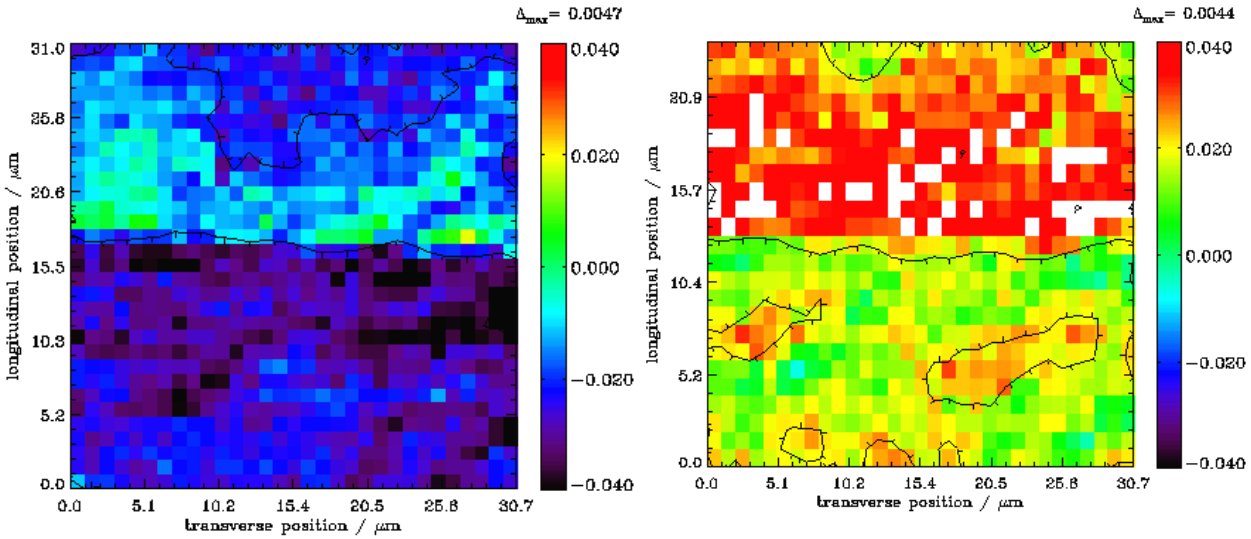

Fig. 2.70. Two-dimensional mappings of a $HoFe_2$ crystal for a field of 0.43 Tesla, applied with opposite orientations. The magnitude of the field was sufficient to align the sample parallel to the applied field. The flipping ratio changed sign.

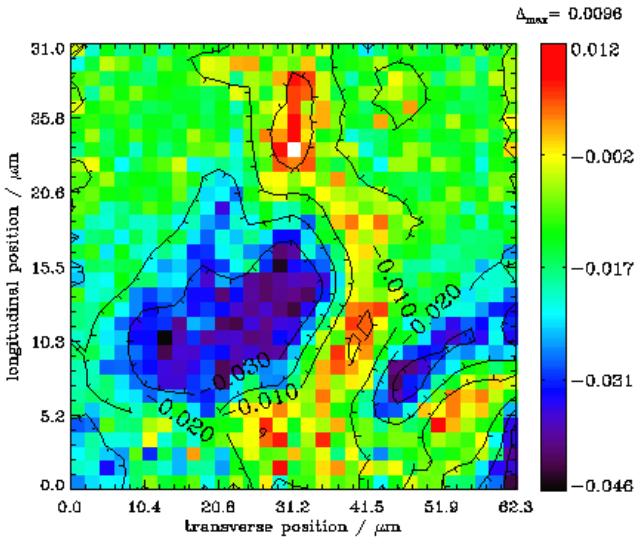

Fig. 2.71. Two-dimensional mapping of the remanent magnetic structure of the $HoFe_2$ crystal. Magnetic domains can be clearly identified.

2.7.2 Temperature Dependence of the X-ray Magnetic Circular Dichroism Signal at the RE L_3 Edge in $REFe_2$

Compounds containing rare earths (RE) and 3d transition metals (TM) are of great technological importance due to the wide range of industrial applications, such as magneto-optical disks, transducers, and most importantly high-performance permanent magnets. In these materials the RE atom is used to increase the magnetic anisotropy, while the transition metal enhances the Curie temperature. The magnetic moment on the RE atom arises primarily from the highly localized 4f orbital, which has negligible overlap with the surrounding atoms, while the moment on the TM arises on the much more delocalized 3d orbital. Thus magnetic ordering in these compounds is mediated through an indirect exchange, whereby the RE 4f orbital spin-polarizes the more diffuse RE 5d orbital, which in turn has a direct exchange coupling with the TM 3d orbital. Clearly for a well-defined understanding of the magnetic properties of these materials, knowledge of the spin-polarization and exchange-coupling mechanisms involved in the 5d orbital is essential.

X-ray magnetic circular dichroism (XMCD) provides an ideal tool for providing just such information. XMCD is defined as the difference in the absorption coefficient between right- and left-handed circularly polarized x-rays. Since wave functions of the initial core levels are well understood, the structure in the measured spectra can be directly correlated to the spin-polarization of the final state orbital allowed by selection rules. Furthermore since the core level binding energies are unique to each of the constituent atoms in a material, the information obtained is specific to a particular element and orbital.

In this report, we present XMCD measurements at the RE L_3 edge on a series of $REFe_2$ compounds (RE = Ho, Er, Tm, Lu). The mechanism behind the magnetic ordering in these materials is the well-known RKKY interaction, illustrated in Fig. 2.72. The well-localized 4f orbital spin-polarizes the 5d orbital via an exchange $\xi_{4f\text{-}5d}$, which in turn interacts with the TM 3d orbital through $\xi_{5d\text{-}3d}$ exchange. Additionally, the TM atoms also have a strong coupling between themselves though a direct overlap of their respective 3d orbitals ($\xi_{3d\text{-}3d}$). Since the direct exchange between the TM atoms $\xi_{TM\text{-}TM}$ ($\sim \xi_{3d\text{-}3d}$) is typically much stronger than the indirect exchange between the RE and TM atoms $\xi_{RE\text{-}TM}$ ($\sim \xi_{4f\text{-}5d} * \xi_{5d\text{-}3d}$), the magnetization of the RE sublattice will fall off faster than that of the TM. Previous XMCD measurements at these edges have

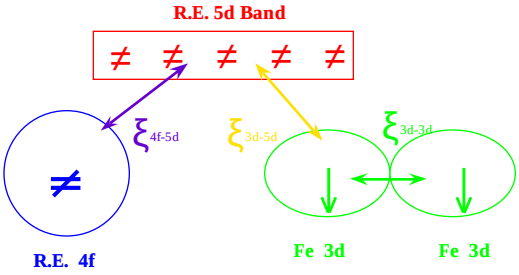

Fig. 2.72. Schematic of the magnetization process.

shown that they are composed of two distinct features. One is associated with the 5d orbital, while another has been shown to arise from transitions to the 4f orbital (Lang et al., 1995). The effect of the different exchange mechanisms on the spin polarization of the individual orbitals can be investigated by varying the RE and changing the temperature of the material. By changing the RE, the strength of the $\xi_{4f\text{-}5d}$ exchange is varied while keeping the $\xi_{5d\text{-}3d}$ exchange constant. In the case of Lu, this exchange goes to zero since it has no 4f moment, thereby isolating effects of the $\xi_{5d\text{-}3d}$ interaction alone. In the temperature behavior, features that are more tightly coupled to the TM lattice should show less temperature variation.

Powder samples were prepared of each material and placed on tapes for transmission measurements. The samples were placed inside a closed loop He displex in order to vary the temperature between 10K and 300K. In order to magnetize the sample, a 4.0 kG permanent magnet was also placed inside the displex. The magnetic field was oriented at 45˚ with respect to the incident beam in order to allow the transmitted beam onto the detector. The entire displex with the magnet and sample inside could be rotated by 180˚ in order to take data with the field both parallel and antiparallel to the incident beam helicity. This eliminated any artifacts in the signal that were not due solely to the sample magnetization. Spectra were taken by reversing the helicity at each energy using a diamond (111) phase retarder.

Figure 2.73 shows the XMCD spectra for each RE compound at 10K and 300K. The spectra of Ho, Er, and Tm each show prominent features at approximately –8 and +4 eV, which are known to come from the 4f and 5d bands, respectively. Lu on the other hand shows a single peak at ~0 eV. A peak at this energy is also clearly seen in the TM spectra at 300K (arrow). Note that the TM spectra inverts with increasing temperature since at room temperature it is above its compensation point. Taking the derivative of the XMCD spectra reveals that this feature is present in both the Er and Ho spectra also but is simply obscured by the

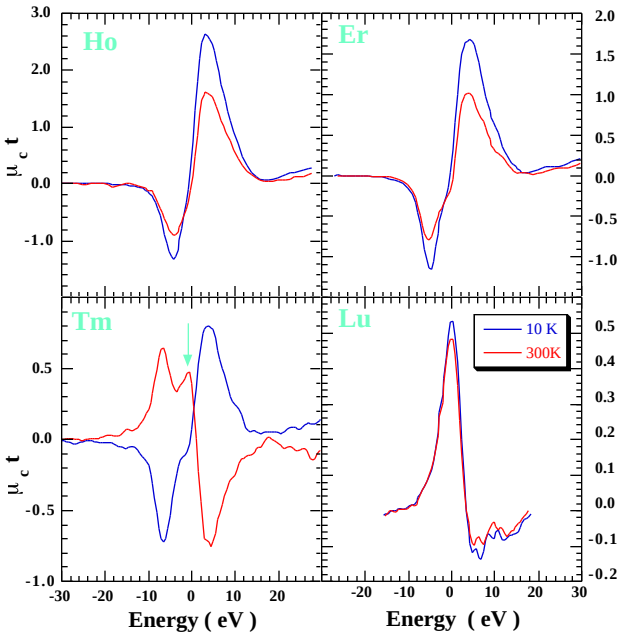

Fig. 2.73. Dichroism signal in RFe_2 at 10K (blue) and 300K (red).

much larger pre- and post-edge features. Clearly since this feature is present in Lu, it must be caused by the $\xi_{5d\text{-}3d}$ interaction. To deconvolute this small feature from the much larger nearby peaks, each spectra was fit using three Gaussian curves. This is shown in Fig. 2.74, which shows data taken at the Er edge along with the three curves used to fit the spectra. The three peaks in the spectra are labeled Q, P, and D. Peak Q is known to be associated with the RE 4f states, while peak D is known to be due to the 5d orbital. The exact nature of peak P is unclear, but as mentioned above (and shown by its temperature dependence below), its most likely source is the exchange between the TM 3d and RE 5d states, since it has nearly the same magnitude and occurs at nearly the same energy as the peak in the Lu spectra.

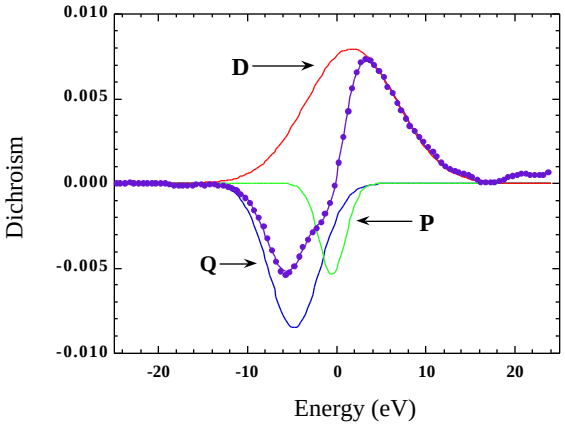

Fig. 2.74. Deconvolution of the dichroism spectra into three Gaussian curves.

The changes in each of the features in the XMCD spectra as a function of temperature are plotted in Fig. 2.75. Also plotted in this figure are single-crystal neutron diffraction measurements (Clark, 1979) of the RE sublattice magnetization for Ho, Er, and Tm. The dotted line on the Lu data is meant merely as a guide to the eye, since no neutron measurements for this material were available. There are several things to notice about the temperature variations in the signal. First the 4f and 5d features have approximately the same temperature dependence. This would indicate that the 5d band polarization probed by feature D scales nearly identically with the 4f magnetization; therefore it is dominated by the $\xi_{4f\text{-}5d}$ exchange, which is consistent with recent theoretical results (van Veenendaal et al., 1997). Feature P, on the other hand, falls off much less with increasing temperature in Ho, Er, and Tm, than the D and Q features, consistent with this feature being strongly associated with the $\xi_{5d\text{-}3d}$ exchange, since it scales with the expected magnetization of the TM sublattice. Lastly, while the D and Q features follow the general trend of the neutron measurements, substantial deviations are seen for the Er and Tm spectra. At

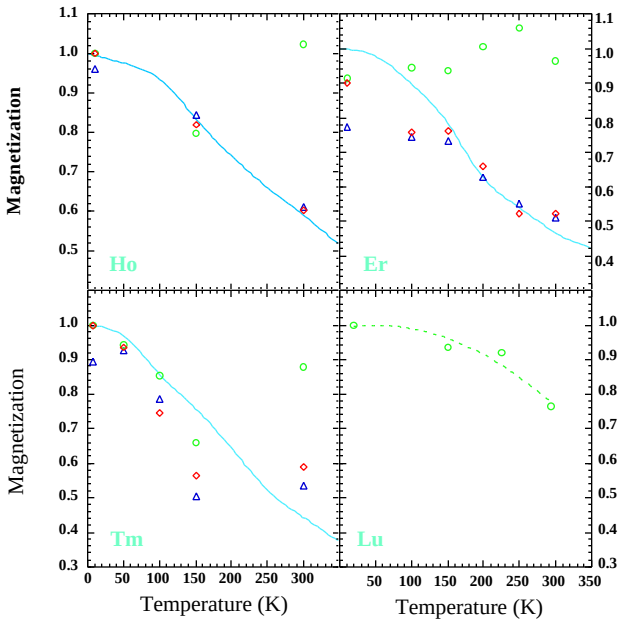

Fig. 2.75. Temperature dependence of each feature in the dichroism spectra [Q (triangle), D (diamond), and P (circles)].

low temperatures the sample becomes much harder to magnetize due to increasing anisotropy, thus the XMCD data tend to deviate away from the neutron data, which were taken on single-crystal samples. Additionally the TM data might be affected by the proximity of some of the measurements to the compensation temperature (T=250K, where the net magnetization is zero).

2.7.3 Interfacial Structure and Magnetism in Fe/Gd Multilayers

Interface structure affects many of the phenomena exhibited by magnetic films and multilayers. Yet even though the importance of interface structure is widely acknowledged, studies to date have generally ignored the magnetic component of the interface structure due to the surface sensitivity of most magnetic probes (e.g., MFM and MOKE). By using a tunable high-brilliance x-ray beam, however, the shortcomings with these techniques can be overcome to obtain information about the magnetic interfaces buried deep in the bulk of a material. Here we describe one such study of the x-ray resonant magnetic scattering (XRMS) in the reflectivity measurements of an Fe/Gd multilayer.

The experimental setup used for the XRMS measurements is shown in Fig. 2.76. A diamond phase retarder is used to convert the linear polarized undulator beam to a circularly polarized one. By alternating the helicity of the beam incident on the sample, the measurements become sensitive to the net magnetization within the sample. Therefore pure charge and charge-magnetic interference information can be extracted

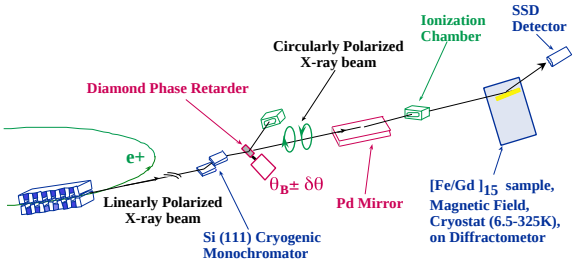

Fig. 2.76. Experimental setup.

from the data by taking the sum and difference of the measurements taken with opposite helicities. The sample was placed inside a closed loop He cryostat, which was then mounted on a 4-circle diffractometer for the reflectivity measurements. A fixed magnetic field could be applied to the sample using a permanent magnet.

Measurements of both the specular and the diffuse reflectivity scattering data have been collected in order to obtain magnetic information about the multilayer. Examples of the charge-magnetic interference reflectivity measured near the Gd L_2 and L_3 edges are shown in Fig. 2.77, while pure charge and charge-magnetic interference diffuse scattering are presented in Fig. 2.78. In all figures, Born approximation (BA) fits (Osgood III et al., 1999; Nelson, 1999) to the data are also displayed.

The fits to specular reflectivity data of the type shown in Fig. 2.77, (Nelson, 1999; Ishimatsu et al., 1999) indicate a direct proportionality between the structural roughness and the range of the Fe-Gd exchange coupling. Fits to the diffuse scattering also provide information about the relationship between the structural and magnetic properties of the multilayer. For example, the fits shown in Fig. 2.78 and fits to additional diffuse data measured from

other Fe/Gd multilayers (Nelson et al., 1999) result in longer correlation lengths for both in-plane and out-of-plane charge-magnetic roughness than for pure charge (or structural) roughness. Additional studies focusing on the temperature and energy dependencies of the XRMS data in the Fe-Gd system are already underway.

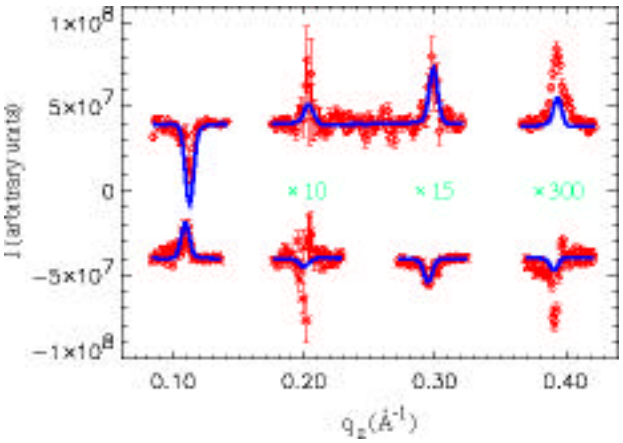

Fig. 2.77. Differences in the specular reflectivity scattering (red) at the Gd L_2 (above) and L_3 (below) edges, along with Born approximation fits (blue) to the data. The data and fit have been shifted by 4x10^7 and enlarged, as labeled, for clarity.

2.7.4 Exploring Magnetic Anisotropy Using Polarized X-rays

As the storage density in magnetic media has increased, so too has the complexity of the materials and structures used. Most technologically relevant magnetic structures now consist of multiple interacting ferromagnetic (FM) layers. However, hysteresis and magnetocrystalline anisotropy are commonly measured using a bulk magnetization techniques. These techniques measure a weighted sum of all the FM elements in the material or device. As a result, interpretation of the data is often

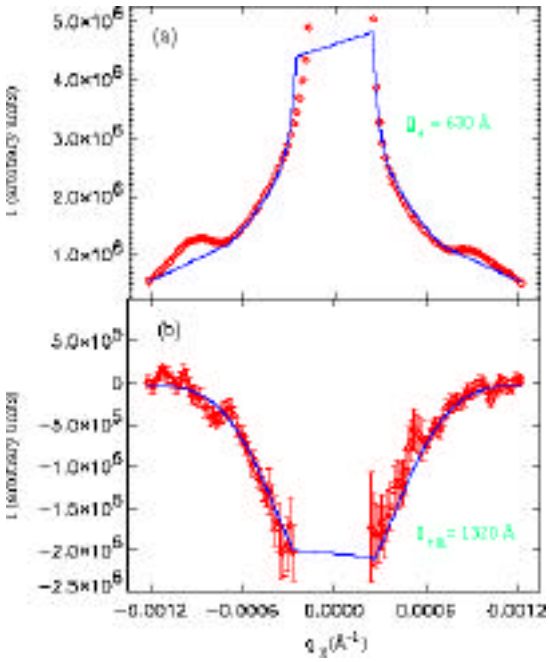

Fig. 2.78. Diffuse scattering (red) from the pure charge(a) and charge-magnetic interference (b), along with BA fits (blue) to the data.

difficult. A solution to this dilemma is to utilize an element-specific technique to separate the individual contribution of each elemental component.

Of particular interest is the study of the magnetic anisotropies that can be accomplished in an element-specific manner using x-ray magnetic linear dichroism (XMLD). XMLD is a magnetic contrast resulting from the slight absorption dependence on the angle between the beam polarization and the magnetic moment. Either by measuring the absorption for the moment and polarization parallel and perpendicular (XMLD) or by measuring the absorption while sweeping the direction of a constant field [referred to as x-ray magnetic linear loops (XMLL)], a wide variety of anisotropy information can be obtained (Fig. 2.79).

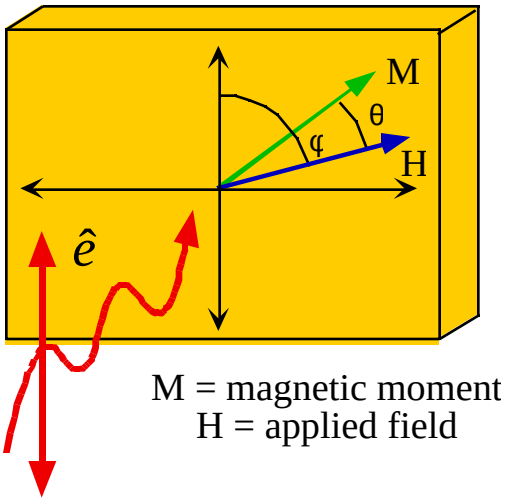

Fig. 2.79. Experimental geometry of the x-ray magnetic linear dichroism measurement. A wide variety of information can be obtained by measuring the absorption for the moment and polarization parallel and perpendicular (XMLD) or by measuring the absorption while sweeping the direction of a constant field [referred to as x-ray magnetic linear loops (XMLL)].

The XMLD observed at the transition metal L edges (see Fig. 2.80) is strongly coupled to the spin-orbit interaction (van der Lann, 1999) making it potentially much better suited to the study of orbital magnetic moment variations. In addition, the spin-orbit interaction is the key link in the connection between the magnetic moment and the lattice that results in the magnetic anisotropy. Strong changes in the line shape are observed by variation in the sample crystal structure and are related to the variation in magnetocrystalline anisotropy. For example, the results for single-crystal bcc Fe(100), shown in Fig. 2.80, are quite distinct from those of polycrystalline Fe (not shown).

Another facet of this technique is the ability to directly probe the symmetry of the magnetic anisotropy. This is accomplished by monitoring the changes in absorption as a

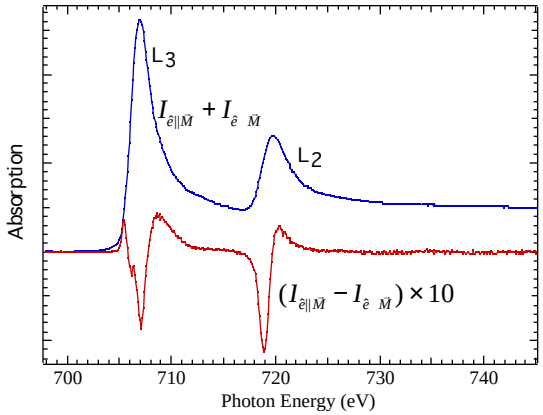

Fig. 2.80. X-ray magnetic linear dichroism for a bcc Fe(100) single crystal displaying the sum and difference spectra. The difference line shape has a strong dependence on crystal order and structure due to changes in the spin-orbit interaction.

constant magnetic field is rotated in the plane of the film (see Fig. 2.81). The comparison of single crystal bcc Fe to that of polycrystalline Fe clearly shows the difference between a 4-fold magneto-crystalline anisotropy to that of no anisotropy. The solid lines show the result of magnetic calculations that through the field magnitude dependence provide quantitative information.

2.7.5 Microspectroscopy and Imaging with Photoelectron Microscopy

With the recent explosion in nano-technology, new techniques are necessary to fully explore the influence of dimensionality on materials. X-ray imaging and micro-spectroscopy are unique tools for the characterization of electronic and magnetic properties. By imaging the secondary electrons emitted due to x-ray excitation with a photoelectron microscope (PEEM), many details of the microstructure can be

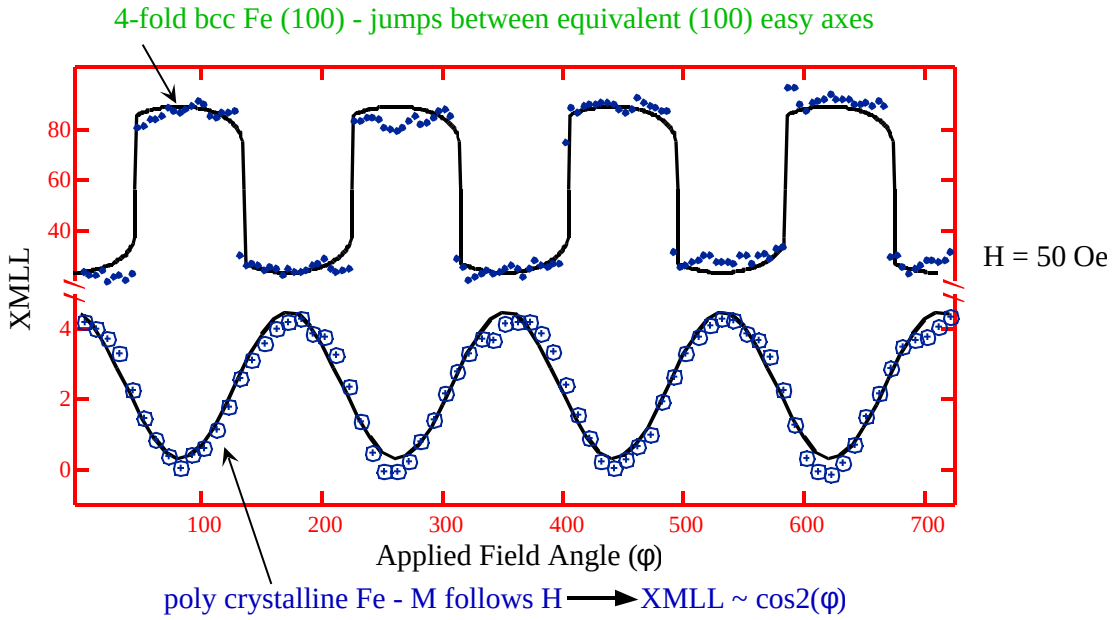

Fig. 2.81. X-ray magnetic linear loops measured by sweeping the in-plane angle of a constant magnetic field amplitude. Results show clear indications of the nature of the magnetocrystalline anisotropy that can be further understood by modeling (solid lines).

.

determined. Figure 2.82 shows an image of 1 µm Pd stripes on Si. In this case the x-ray energy is off resonance and the contrast is due solely to the differing electron density of the two materials. This test sample was utilized to judge the resolution during the recent commissioning of the microscope. By adjusting the optics to optimize for the highest resolution, we could resolve features in the 100 – 200 nm range.

The unique capability of PEEM is not only the ability to image, but the ability to use image intensity to track resonant phenomena and perfom microspectroscopy. Micro-fabrication techniques have enabled production of small-scale structures for technological applications. Figure 2.83 shows a 2 µm NiFe wire prepared as a prototype for nonvolatile magnetic memory elements. Element-specific maps help us

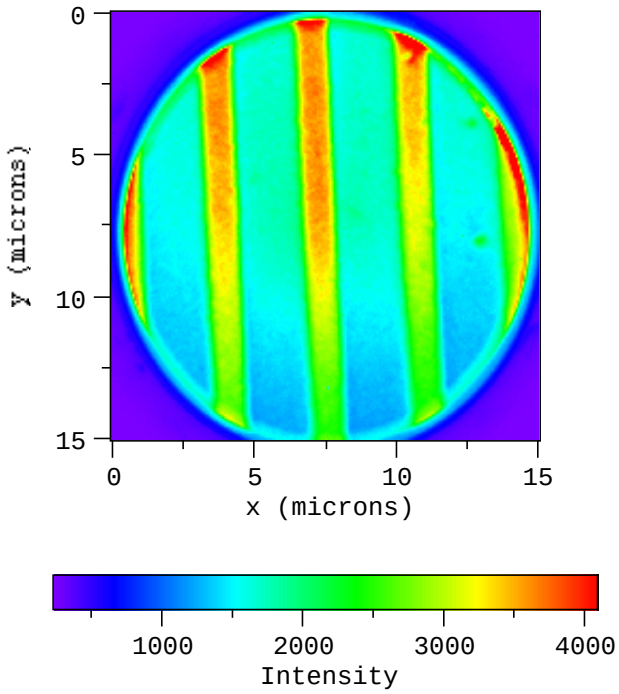

Fig. 2.82. X-ray photoelectron image of 1 µm Pd stripes on a Si wafer. This image displays a 15 µm field of view and was acquired with a 12 bit CCD camera.

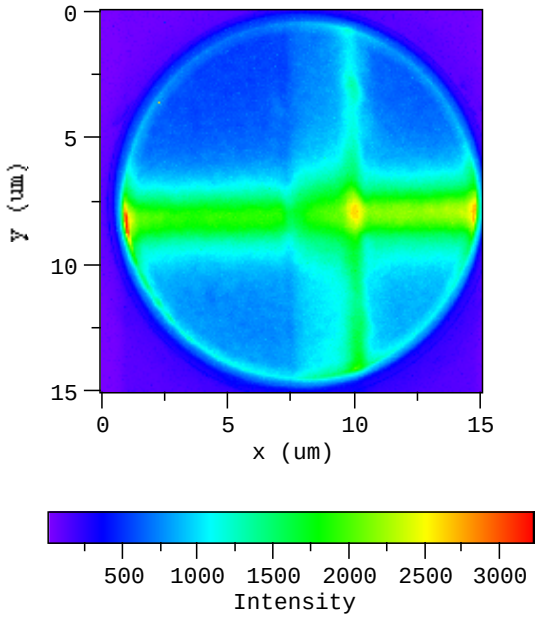

Fig. 2.83. Element-specific image of a 2-µm-wide NiFe magnetic wire with the x-ray excitation energy tuned to the Ni L_3 edge. Future capabilites in sector 4 will enable not only chemical maps, but also magnetic domain structure from polarization-dependent absorption.

understand the production process and can help us identify problems. Electronic structure can be studied by monitoring different parts of the image to track local changes in the absorption (shown in Fig. 2.84). These results show the prescence of oxide contamination in the wire. Another unique feature of the result is the disparity of the local and total absorption. The enhanced absorption lines can be attributed to the coherent nature of the undulator light source that results in a modification of the absorption spectrum (Hunter Dunn et al., 2000). Future work will include study of the coherent excitation process, as well as polarization-dependent studies of magnetic microstructures.

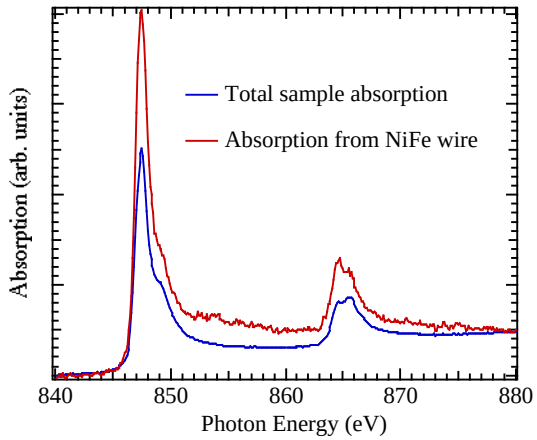

Fig. 2.84. Comparison of total sample absorption, which contains 20 memory elements, to a selected 1 µm x 1µm region of the single element shown in Fig. 2.83. Clear deviations of the absorption from that of metal standards indicate a significant oxide component.

2.7.6 X-ray-Excited Optical Luminescence Studies of Oxidized Porous Silicon

Porous silicon luminescence has attracted considerable attention for application in Si-based optoelectronics (Canham, 1990). However, recent results have been unclear as to the origin of particular luminescence bands. Depending on the study, they can be attributed to either nanocrystals or oxides. To clarify this issue, a study of porous silicon as a function of oxidation conditions was undertaken. By using x-ray-excited optical luminescence, one can understand the oxide dependence by comparing the results of total x-ray fluorescence yield (TFY) to that of either total or partial luminescence yield (TLY and PLY). Figure 2.85 shows the influence of oxidation on the luminescence that provides clear evidence for overlapping luminescence bands from both Si nanocrystals and oxides. These

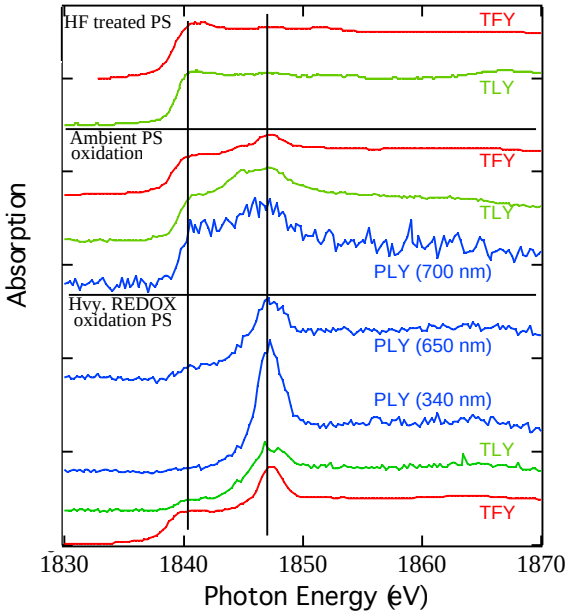

Fig. 2.85. Comparison of total fluorescence yield (TFY) to that of total and partial luminescence (TLY and PLY) as a function of oxidation. Changes in the luminescence yield for the oxide peak near 1847 eV with respect to that of the pure Si peak near 1840 eV provide clear evidence for overlapping luminescence bands from both Si nanocrystals and oxides.

overlapping bands are the cause of much of the confusion in the literature, and x-ray-excited optical luminescence is uniquely suited to extracting element, as well as chemical-state-specific, information for optical materials.

In addition to optical yields, this technique can also directly provide information on the shape of the optical bands. By using an optical monochromator for fixed photon excitation energies, one can follow the evolution of the emission bands (see Fig. 2.86). Future studies will utilize these bands to understand the interaction of local structure and the optical luminescence.

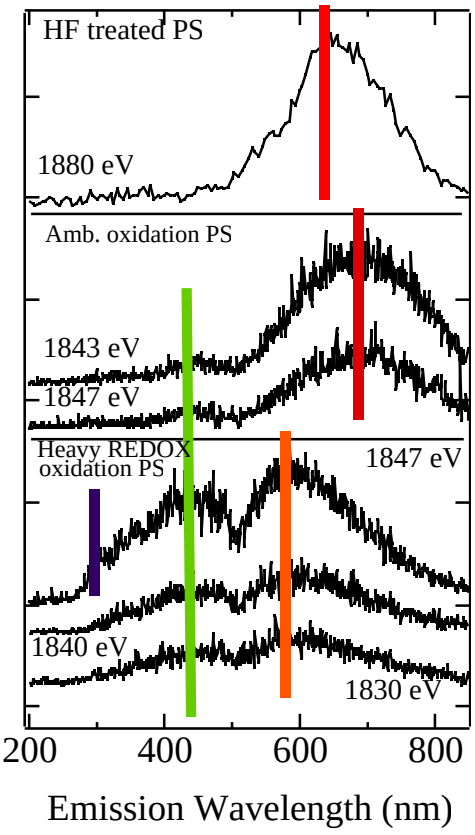

Fig. 2.86. Optical emission spectra as a function of both oxidation and photon energy.

As well, the polarization source becoming available in sector 4 this fall will open the door to element-specific studies of magneto-optical materials.

2.7.7 Changes of a Ferromagnet/ Insulator Interface upon Thermal Annealing

Recent success in fabrication of magnetic tunneling junctions (MTJ) with magneto-resistance (MR) above 40% at room temperature has generated a great deal of interest due to potential application as efficient magnetic random access memory (MRAM) (Parkin et al., 1999). MTJs are composed of two FM electrodes separated by an insulating layer (I) with typical

structures being CoFe/ Al_2O_3/CoFe. Others have reported that these record high MR values are obtained only after annealing the MTJ to 200-300ºC, which leads to ~10% increase in MR when compared with as grown structures (Parkin et al., 1999). It is suspected that the oxidation of the Al overlayer penetrates into the CoFe underlayer and is subsequently removed by annealing. To understand the influence of annealing x-ray absorption spectroscopy (XAS) was used to directly monitor the chemical states of FM in a $Co_{84}Fe_{16}/Al_2O_3$ bilayer before and after the annealing process. XAS at the L_3-edge of 3d transition metal elements and their oxides exhibit different, easily distinguishable features, which makes it an ideal tool for investigating the oxidation states of FM electrodes in MTJ.

A bilayer consisting of an Al wedge was used in order to perform a systematic study of the effect of annealing as a function of Al_2O_3 thickness (see Fig. 2.87). This is of particular importance since the Al_2O_3 barriers of MTJ are fabricated by oxidation of Al layers and an optimal FM/I interface

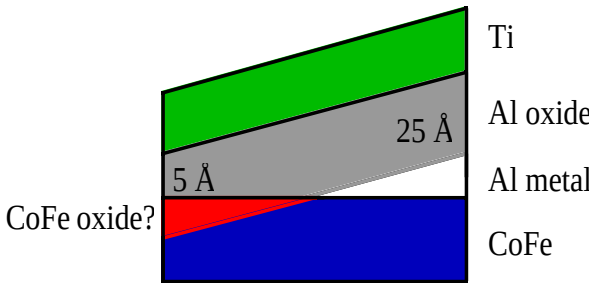

Fig. 2.87. Wedge-shaped structure used to study the Al layer thickness dependence of the oxidation process. CoFe oxide removal upon annealing is suspected to be responsible for improved magnetoresistance.

should have all of the Al and none of the FM oxidized. Absorption at the Co L edge clearly shows pre-edge features indicative of an oxide. By tracking the intensity of this feature as a function of both Al layer thickness and annealing, one can see that there is significant removal of the oxide upon annealing (see Fig. 2.88). In addition the Al K edge absorption spectra show little variation with annealing and are indicative of a disordered Al oxide.

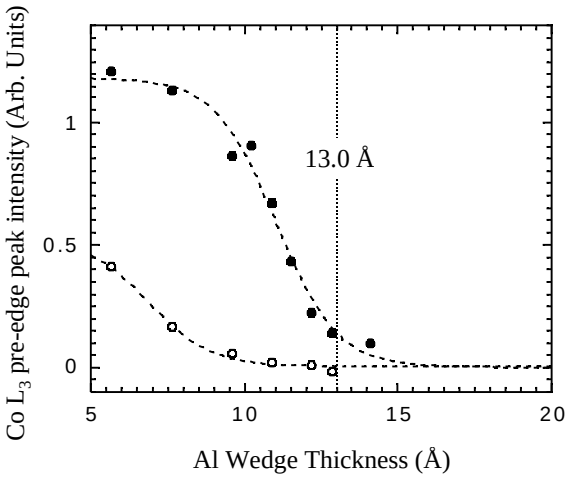

Fig. 2.88. Co pre-edge feature intensity as a function of Al thickness before (closed circles) and after annealing (open circles). Heating drives the oxygen out of the CoFe layer and results in an improved interface and subsequently improved magnetoresistance.